STEM CELLS TRANSLATIONAL MEDICINE®

TISSUE ENGINEERING AND REGENERATIVE MEDICINE

Integration and Regression of Implanted Engineered Human Vascular Networks During Deep Wound Healing

DONNY HANJAYA-PUTRA,[a] YU-I SHEN,[a] ABIGAIL WILSON,[a] KAREN FOX-TALBOT,[b] SUDHIR KHETAN,[c] JASON A. BURDICK,[c] CHARLES STEENBERGEN,[b] SHARON GERECHT[a]

Key Words. Endothelial progenitors • Angiogenesis • Tissue regeneration • Hyaluronan • Wound healing • Vascular engineering • Hydrogel • Microvasculature

[a]Department of Chemical and Biomolecular Engineering, Johns Hopkins Physical Sciences-Oncology Center and Institute for NanoBioTechnology, Johns Hopkins University, Baltimore, Maryland, USA; [b]Department of Pathology, Johns Hopkins University School of Medicine, Baltimore, Maryland, USA; [c]Department of Bioengineering, University of Pennsylvania, Philadelphia, Pennsylvania, USA

Correspondence: Sharon Gerecht, Ph.D., Department of Chemical and Biomolecular Engineering, Materials Science and Engineering, Johns Hopkins Physical Sciences-Oncology Center and Institute for NanoBioTechnology, Johns Hopkins University, 3400 North Charles Street, Baltimore, Maryland 21218, USA. Telephone: 410-516-2846; Fax: 410-516-5510; E-Mail: gerecht@jhu.edu

Received September 2, 2012; accepted for publication January 3, 2013; first published online in SCTM *EXPRESS* March 13, 2013.

1066-5099/2013/$20.00/0

http://dx.doi.org/10.5966/sctm.2012-0111

ABSTRACT

The ability of vascularized constructs to integrate with tissues may depend on the kinetics and stability of vascular structure development. This study assessed the functionality and durability of engineered human vasculatures from endothelial progenitors when implanted in a mouse deep burn-wound model. Human vascular networks, derived from endothelial colony-forming cells in hyaluronic acid hydrogels, were transplanted into third-degree burns. On day 3 following transplantation, macrophages rapidly degraded the hydrogel during a period of inflammation; through the transitions from inflammation to proliferation (days 5–7), the host's vasculatures infiltrated the construct, connecting with the human vessels within the wound area. The growth of mouse vessels near the wound area supported further integration with the implanted human vasculatures. During this period, the majority of the vessels (~60%) in the treated wound area were human. Although no increase in the density of human vessels was detected during the proliferative phase, they temporarily increased in size. This growth peaked at day 7, the middle of the proliferation stage, and then decreased by the end of the proliferation stage. As the wound reached the remodeling period during the second week after transplantation, the vasculatures including the transplanted human vessels generally regressed, and few microvessels, wrapped by mouse smooth muscle cells and with a vessel area less than 200 μm^2 (including the human ones), remained in the healed wound. Overall, this study offers useful insights for the development of vascularization strategies for wound healing and ischemic conditions, for tissue-engineered constructs, and for tissue regeneration. STEM CELLS TRANSLATIONAL MEDICINE *2013;2:297–306*

INTRODUCTION

Successful regeneration of many injured and diseased tissues requires timely vascularization to supply the necessary nutrients and oxygen to support the renewal and differentiation of new tissues [1]. The survival of tissue-engineered organs during transplantation depends on rapid vascularization and anastomosing with the host's vasculature [2, 3]. One promising approach is the transplantation of fully functionalized microvascular networks that can rapidly integrate with the host's circulatory system [3–5]. Many studies have used natural matrices, such as collagen, fibrin, and Matrigel (BD Biosciences, San Diego, CA, http://www.bdbiosciences.com), to study the prevascularization potential of various human stem cells, including embryonic stem cell-derived endothelial cells [6–8], endothelial progenitor cells (EPCs) [9, 10], endothelial colony-forming cells (ECFCs) [11, 12], and mesenchymal stem cells [9, 13]. However, the inherent chemical and physical properties of these natural materials have limited their clinical usage [14, 15]. Recent studies have explored synthetic materials as a xeno-free and more clinically relevant alternative for both therapeutic angiogenesis [16, 17] and vascularization of tissue-engineered constructs [18, 19]. We recently reported that hyaluronic acid (HA) hydrogels can be engineered to precisely control the generation of functional human vascular networks by ECFCs [20]. Using engineering design parameters, we also controlled vascular morphogenesis with spatial precision [21].

Thermal wounds caused by third-degree burns heal slowly, because of damage to both epidermal and dermal layers, as well as trauma to the underlying muscles, bones, and tendons [22]. The healing process involves three main stages: inflammation, proliferation, and remodeling [23]. In the inflammation stage, neutrophils flow into the wound area and clear cellular and foreign debris, followed by macrophages, which produce cytokines that induce angiogenesis [22]. During the overlap between the inflammation and proliferation stages,

an eschar forms on the surface of the wound. During the proliferation stage, new vessels form through vasculogenesis, from bone-marrow progenitors as well as through angiogenesis, from the surrounding vascular bed [24, 25]. These vessels support the growing new tissues and are critical in determining the wound-healing outcome [26, 27]. Once the wound reaches the remodeling stage, epidermis fully covers the wound, collagen becomes crosslinked, and vascular networks get pruned [22, 28]. Promoting angiogenesis during the healing process of third-degree burns has been shown to promote dermal layer regeneration and complete skin regeneration [29]. For patients with vascular insufficiency (e.g., diabetics and the elderly), third-degree burns can lead to chronic, nonhealing wounds or ulcers. Schechner and colleagues [30, 31] pioneered the use of marrow-derived circulating EPCs to promote vascularization prior to skin graft transplantation. After ex vivo culture of EPCs on the collagen-based skin graft, EPCs revascularized and promoted the survival of the skin grafts with minimal immune response [32]. More recently, putative EPCs have been redefined as ECFCs to underscore their stem cell properties, including their robust proliferative potential, their ability to form secondary and tertiary colonies, and their capacity, in vivo, to form blood vessels de novo [33, 34].

The hypothesis of the current study was that human-engineered vasculature beds from ECFCs in a synthetic matrix localize and integrate with the host's vessels during the process of deep-wound healing in mice. We used third-degree burn wounds as our pathological model of choice because of its wide clinical implications [29]. We investigated the survival of human vascular networks within severely injured tissues, the kinetics of engineered human microvasculature integrating with the host blood vessels, and their functionality and durability during the healing of the burned wound.

Materials and Methods

Human ECFCs

ECFCs, from human umbilical cord blood isolated from outgrowth clones (kindly provided by Dr. Mervin C. Yoder, Indiana University School of Medicine) were expanded in endothelial growth media (EGM; PromoCell, Heidelberg, Germany, http://www.promocell.com) and used for experiments between passages 6 and 8, as previously described [34, 35].

Synthesis of Acrylated HA Hydrogels

Acrylated HA (AHA) hydrogels were prepared as previously reported [36, 37]. Briefly, AHA was synthesized using a two-step protocol: (a) the tetrabutylammonium salt of HA (HA-TBA) was formed by reacting sodium hyaluronate (64 kDa; Lifecore Biomedical, Chaska, MN, http://www.lifecore.com) with the highly acidic ion exchange resin Dowex-100 and neutralizing with 0.2 M tetrabutylammonium hydroxide; (b) acrylic acid (2.5 Eq) was coupled to HA-TBA (1 Eq, repeat unit) in the presence of dimethylaminopyridine (0.075 Eq) and di-*tert*-butyl dicarbonate (1.5 Eq) in dimethyl sulfoxide, followed by dialysis and lyophilization. ^{1}H NMR was used to confirm the final percentage of modification of the AHA.

Peptides

The cell adhesive peptide GCGYG***RGD***SPG (molecular weight, 1,025.1 Da; bold italic type indicates the RGD integrin-binding domain) and matrix metalloproteinase (MMP)-sensitive crosslinker GCRDGPQG ↓ IWGQDRCG (molecular weight, 1,754.0 Da; down arrow indicates the site of proteolytic cleavage) were obtained from GenScript (Piscataway, NJ, http://www.genscript.com), all with more than 95% purity (per manufacturer high-performance liquid chromatography analysis).

ECFC Encapsulation and Culture

AHA polymer (3 wt%) was dissolved in sodium phosphate-buffered saline (NaPBS buffer: 0.1 M sodium phosphate, 0.3 M total osmolarity, pH 8.0). The cell adhesive peptides (RGDS; GenScript) were dissolved in NaPBS buffer and added to the AHA solution at a final peptide concentration of 3.7 mM and allowed to react for 1 hour with gentle shaking. Recombinant human vascular endothelial growth factor 165 (Pierce, Rockford, IL, http://www.piercenet.com), basic fibroblast growth factor (Invitrogen, Carlsbad, CA, http://www.invitrogen.com), Ang-1 (R&D Systems Inc., Minneapolis, MN, http://www.rndsystems.com), tumor necrosis factor-α (R&D Systems Inc.), and stromal cell-derived factor-1 (R&D Systems Inc.) were added at 50 ng/ml into the AHA-RGDS mixture. Human umbilical cord blood ECFCs were encapsulated in HA hydrogels at a density of 5×10^6 cells per milliliter. Following the resuspension of cells into this solution, MMP peptide crosslinker (MMP; GenScript) dissolved in NaPBS buffer was added at 4.83 mM (corresponding to the 25% of available acrylate groups within the 3 wt% AHA). Immediately after adding the MMP crosslinker, 50 μl of this mixture was pipetted into sterile molds (5-mm diameter, 2-mm height) and allowed to react for 15 minutes at room temperature inside the laminar flow hood. The formed constructs were cultured for up to 3 days in EGM (PromoCell). Visualization and image acquisition were performed using an inverted light microscope (IX50; Olympus, Center Valley, PA, http://www.olympusamerica.com) and a confocal microscope (LSM 510 Meta; Carl Zeiss, Jena, Germany, http://www.zeiss.com) at various times during culture.

Transplantation of Vascularized Constructs in a Burn-Wound Model

Vascularized constructs were implanted into the posterior dorsum of 6- to 8-week-old nude mice with burn injuries, following well-established protocols [29, 38]. Briefly, the mice were anesthetized with isoflurane (Thermo Fisher Scientific, Rockville, MD, http://www.thermofisher.com), the dorsum was shaved, a depilatory was applied (Nair; Church & Dwight Co., Inc., Princeton, NJ, http://www.churchdwight.com), and a burn injury was generated using a custom-made 220-g aluminum rod heated in a 100°C water bath for 5 minutes. A template (1.2 cm in diameter) was used to place the wound on the posterior dorsum of each mouse for 4 seconds. Following current clinical practice, we performed burn-wound excision after 48 hours, removing full-thickness skin and generating a round wound (8 mm in diameter) that was covered with vascularized constructs of the same size that had been cultured in vitro for 3 days (one construct per mouse). The wound was then covered with DuoDerm dressing (ConvaTec, Skillman, NJ, http://www.convatec.com). Eight to ten constructs were implanted for each group. At each time point, as described below, human specific fluorescein-conjugated *Ulex europaeus I* (*UEA-I*) *Lectin* (1:10; Vector Laboratories, Burlingame, CA, http://www.vectorlabs.com) and mouse-specific rhodamine-conjugated *Isolectin Griffonia simplicifolia* (*GS*)-IB_4 (1:10; Invitrogen) were injected through the tail veins of the mice [12]. After 20 minutes, the mice were euthanized, and the constructs were harvested and fixed in 3.7% formaldehyde (Sigma-Aldrich, St. Louis, MO, http://www.sigmaaldrich.com). After visual inspection, the tissue was processed for histology. The Johns Hopkins

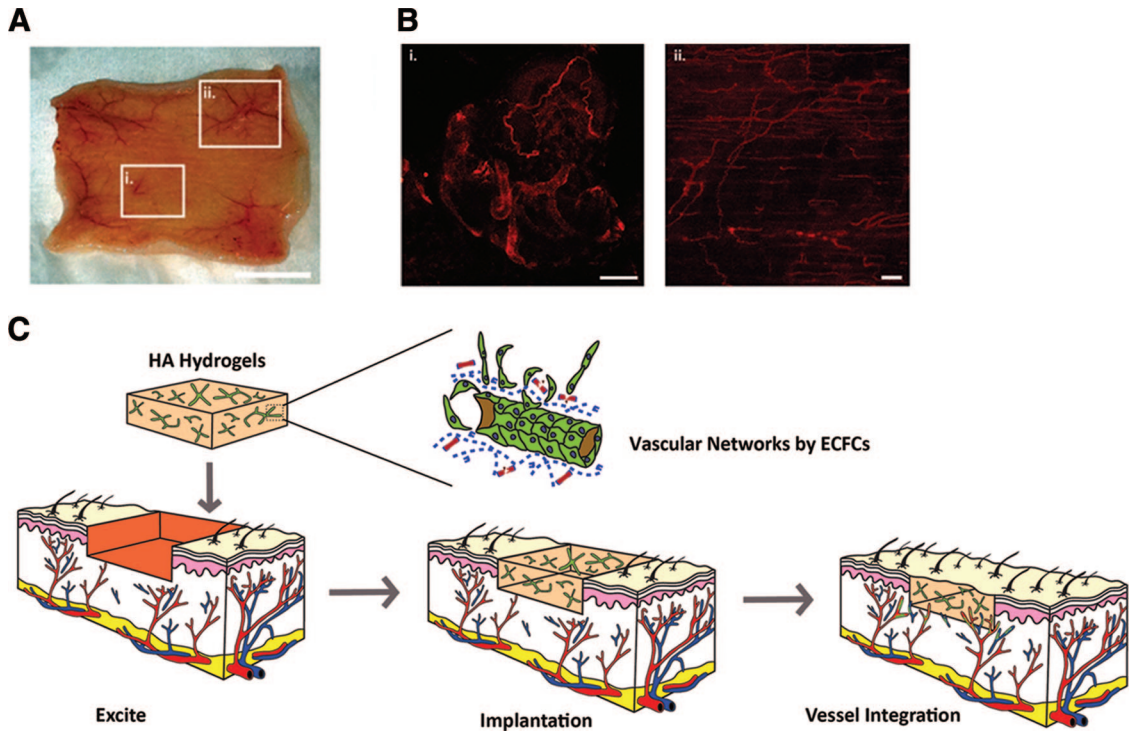

Figure 1. Skin injury and implantation strategy. Burn injuries were generated as previously described [29], followed by wound excisions of full-thickness skin. **(A):** This representative image of excised skin shows the burn area with skin trauma and disturbed blood vessels **(Ai)** compared with an unwounded area with normal blood vessels **(Aii)**. Scale bar = 10 mm. **(B):** Rhodamine-conjugated *GS-IB4* lectin was perfused prior to the excision to label the mouse vasculature networks. Representative confocal images show the vessels at the burned area **(Bi)** compared with the unwounded area **(Bii)**. Scale bars = 100 μm. **(C):** Schematic of study strategy. The wounds were treated with HA hydrogels with human vascular networks from ECFC to analyze the integration of the human and host vascular networks during the healing process. Abbreviations: ECFCs, endothelial colony-forming cells; HA, hyaluronic acid.

University Institutional Animal Care and Use Committee approved all animal protocols.

Histology and Immunohistochemistry

Following fixation of construct explants, the samples were dehydrated in graded ethanol (70%–100%), embedded in paraffin, serially sectioned using a microtome (5 μm), and treated with hematoxylin and eosin (H&E) stain or Masson's trichrome stain or immunoperoxidase stains for anti-mouse F4/80 (Life Technologies, Rockville, MD, http://www.lifetech.com), anti-mouse α-smooth muscle actin (α-SMA) (Abcam, Cambridge, U.K., http://www.abcam.com), or anti-human CD31 (Dako, Glostrup, Denmark, http://www.dako.com) [20, 39]. Double staining was performed using the same anti-human and anti-mouse α-SMA followed by conjugation with anti-mouse Alexa Fluor 488 (Life Technologies) or anti-rabbit Alexa Fluor 594 (Life Technologies), and couterstained with 4′,6-diamidino-2-phenylindole (Life Technologies) as previously reported [40]. Appropriate IgG isotypes were used as previously reported [20].

Statistical Analysis

Having sampled a minimum of six images for each construct, the number and sizes of mouse vessels (α-SMA-positive vessels), human vessels (human CD31-positive vessels), and human vessels wrapped by mouse smooth muscle cells (SMCs; vessels double positive for human CD31 and mouse-α-SMA) were counted, measured, and normalized to tissue area. The wound area was photographed and measured throughout the progression of the wound-healing period and normalized to the wound area at the initiation of the wound. Degradation was determined by fragments of hydrogels as observed in H&E- and F4/80-stained slides [29, 41]. Skin thickness was determined by measuring the epidermis, dermis, and fat tissue in Masson's trichrome-stained histologic sections [29]. Statistical analysis was performed using GraphPad Prism 4.02 (GraphPad Software, Inc., San Diego, CA, http://www.graphpad.com). *t* tests were performed to determine significance using GraphPad Prism 4.02. Significance levels were set at $p < .05$ (*) and $p < .01$ (**). All graphical data were reported.

Results

Implanting Engineered Human Vascular Networks in Third-Degree Burn Wounds

We previously reported that HA hydrogels can be engineered to support functional human microvascular networks with ECFCs [20, 21]. Here, we sought to determine whether engineered human microvascular networks within the HA hydrogels could survive implantation into severely injured tissue, localize, and integrate with the host's vasculature to supply blood to the healing tissue. In pursuit of translational outcomes, we used a third-degree burn-wound model and a procedure we previously developed for applying hydrogels onto burn wounds in mice [29]. Such a deep thermal wound traumatizes the underlying skin and vasculature (Fig. 1A). This trauma results in dead tissues and regressed and distorted vasculature (Fig. 1Bi) compared with normal vasculature (Fig. 1Bii). Current clinical practice excises these dead tissues

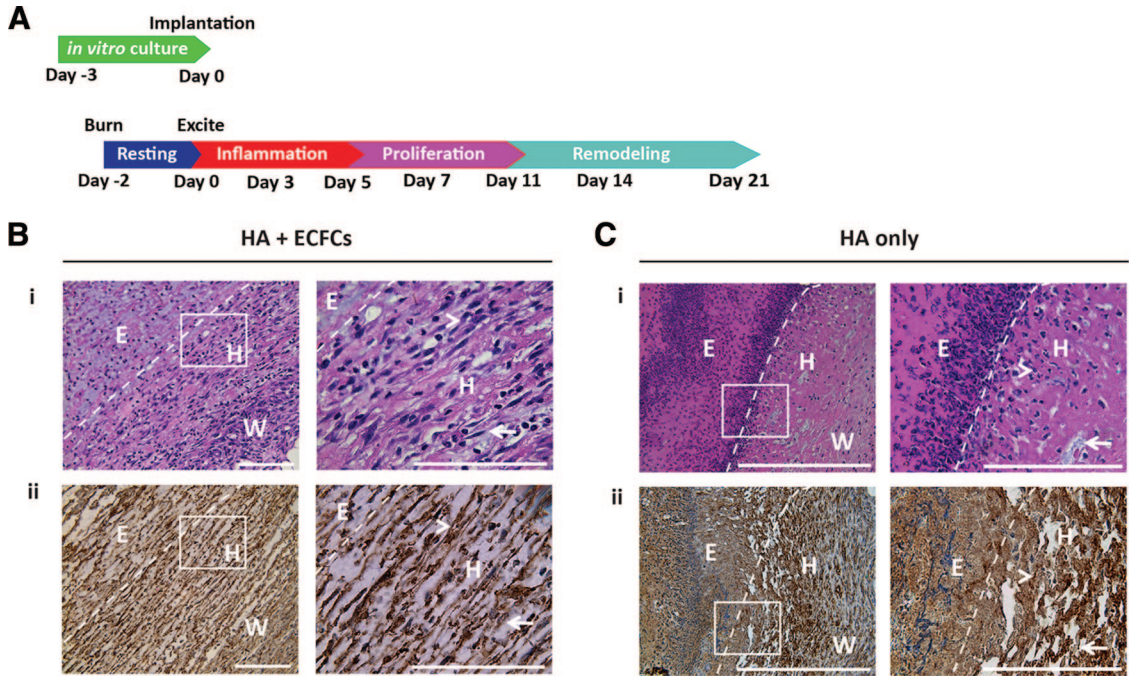

Figure 2. Timeline analysis and the inflammation period. **(A):** Timeline of the study, including the generation of human vascular networks in vitro (day −3), generation of the third-degree burn model (day −2), and implantation of the constructs (day 0). The vascular integration kinetics were followed throughout the healing process: inflammation (day 3), inflammation to proliferation (days 5–7), proliferation to remodeling (days 11–14), and later remodeling (day 21). **(B, C):** HA hydrogels with human vasculature **(B)** and HA hydrogel alone **(C)** (without the addition of any growth factors) were harvested and analyzed after 3 days using H&E-stained histological sections **(Bi, Ci)** and immunohistochemistry for F4/80 mouse macrophage staining **(Bii, Cii)** (brown; counterstain in blue). High magnifications of the boxed areas are shown on the right. The images also show host tissue ingrowth (some indicated by arrowheads) and gel fragmentation (some indicated by arrows). The dotted white lines indicate the boundaries between the eschars and the hydrogels. Scale bars = 100 μm. Abbreviations: E, eschar; ECFCs, endothelial colony-forming cells; H, hydrogel; HA, hyaluronic acid; W, wound.

caused by thermal trauma 2 days after the injury occurs [29]. Thus, we removed dead skin tissue (approximately 8 mm) from the center of the wound, leaving a small (approximately 2 mm) rim of burned tissue around the excision. Meanwhile, we generated in vitro constructs of human vascular networks in the hydrogels; these constructs, similar in shape and size to the burn wound, were then applied to cover the wound (Fig. 1C; supplemental online Fig. 1). To enable placement of the hydrogel construct, protect it from infection, and prevent it from drying, we then layered it with DuoDerm, an ultra-thin dressing [29]. We noticed that the HA hydrogels with vascularized constructs and the HA hydrogel alone (without the addition of any growth factors) mediated wound closure and contraction better than the control, which had no hydrogel (i.e., an excised wound closed with DuoDerm only; data not shown). We hypothesized that human-engineered vasculature would integrate with the host vessels within this wound area.

To test this, we followed the integration kinetics of the human vasculature during the progression in wound healing from the inflammation stage (day 3), through the transitions from inflammation to proliferation (days 5–7) and from proliferation to remodeling (days 11–14), and to the late remodeling stage (day 21; Fig. 2A).

Inflammation Period (Day 3)

At the peak of the inflammation period (day 3), we observed that both HA hydrogels having engineered human vasculature from ECFCs (Fig. 2Bi) and HA hydrogels alone without the addition of any growth factors (Fig. 2Ci) were mostly degraded and replaced by host tissue (Figs. 2B, 2C). Macrophages degraded both the HA hydrogels with engineered human vasculature with ECFCs (Fig. 2Bii) and HA hydrogels alone (Fig. 2Cii). At this stage, human CD31-positive cells were observed within the degraded HA hydrogels around the wound, but they were not perfused with red blood cells (supplemental online Fig. 2A). At the later stages, after the inflammation period, we noticed that hydrogels had been mostly degraded and replaced by the ingrowth of host tissue and vessel network (supplemental online Fig. 3). Thus, beyond this inflammation period, we focused our analysis on the integration kinetics of the engineered vessels.

Inflammation to Proliferation Period (Days 5–7)

At the end of the inflammation period (day 5), we observed many microvessels perfused with red blood cells near the boundary between eschars and hydrogel areas (Fig. 3Ai). Some of these vessels were positive for human CD31 (Fig. 3Aii) and were stabilized by SMCs as indicated by α-SMA-positive staining (Fig. 3Aiii) and double staining for human CD31 and mouse α-SMA (Fig. 3Aiv). A perfusion study illustrated the dynamic interaction between the human vasculature stained with fluorescein-conjugated *UEA-1* lectin (human) and host vasculature stained with rhodamine-conjugated *GS-IB4* lectin (mouse), revealing that the transplanted human vascular networks were functional and anastomosing with the hosts' circulatory systems. Moreover, occasional chimeric vessels were detected that were positive for both human- and mouse-specific lectins (Fig. 3Av). On day 7, the wound areas had larger vasculature (Fig. 3Bi), including vessels

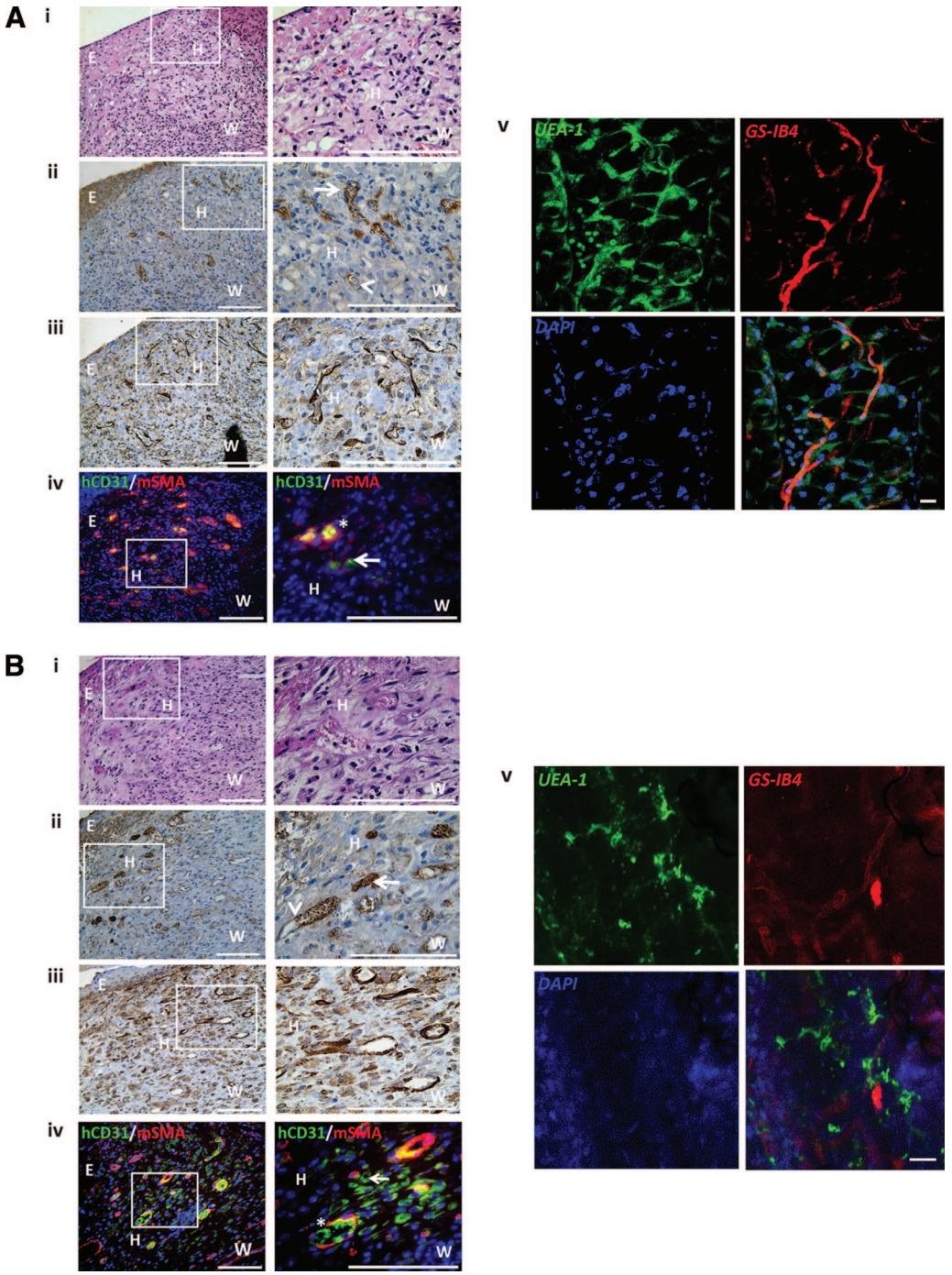

Figure 3. Wound analysis during inflammation to proliferation periods (days 5–7). After treatment with human microvascular constructs, the wounds were analyzed at day 5 **(A)** and day 7 **(B)**. Representative images of H&E-stained histological sections **(Ai, Bi)**, immunohistochemistry for human CD31 staining **(Aii, Bii)** (brown; counterstain in blue), immunohistochemistry for mouse α-SMA staining **(Aiii, Biii)** (brown; counterstain in blue), and immunofluorescence staining for human CD31 (green) and mouse α-SMA **(Aiv, Biv)** (red; nuclei in blue) are shown. High magnifications of the boxed areas are shown on the right. **(Av, Bv):** Representative confocal images of preperfused explant with fluorescein-conjugated *UEA-1* lectin in green; *GS-IB4* lectin in red; nuclei in blue. Human microvasculatures alone (some indicated by arrows), chimeric human and mouse vessels (some indicated by arrowheads), and human microvasculatures wrapped by mouse smooth muscle cells (some indicated by asterisks) are shown. Scale bars = 100 μm. Abbreviations: DAPI, 4′,6-diamidino-2-phenylindole; E, eschar; H, hydrogel; mSMA, mouse α-smooth muscle actin; W, wound.

positive for human CD31 (Fig. 3Bii), other vessels positive for α-SMA (Fig. 3Biii), and double positive for human CD31 and mouse α-SMA (Fig. 3Biv). Perfusion studies showed the interaction between human vascular networks and the host vasculature (Fig. 3Bv).

Proliferation to Remodeling Period (Days 11–14)

At the end of the proliferation stage (day 11), the new, growing tissue became thicker and was supported by large vascular networks (Fig. 4Ai). Some of these large vessels were positive for

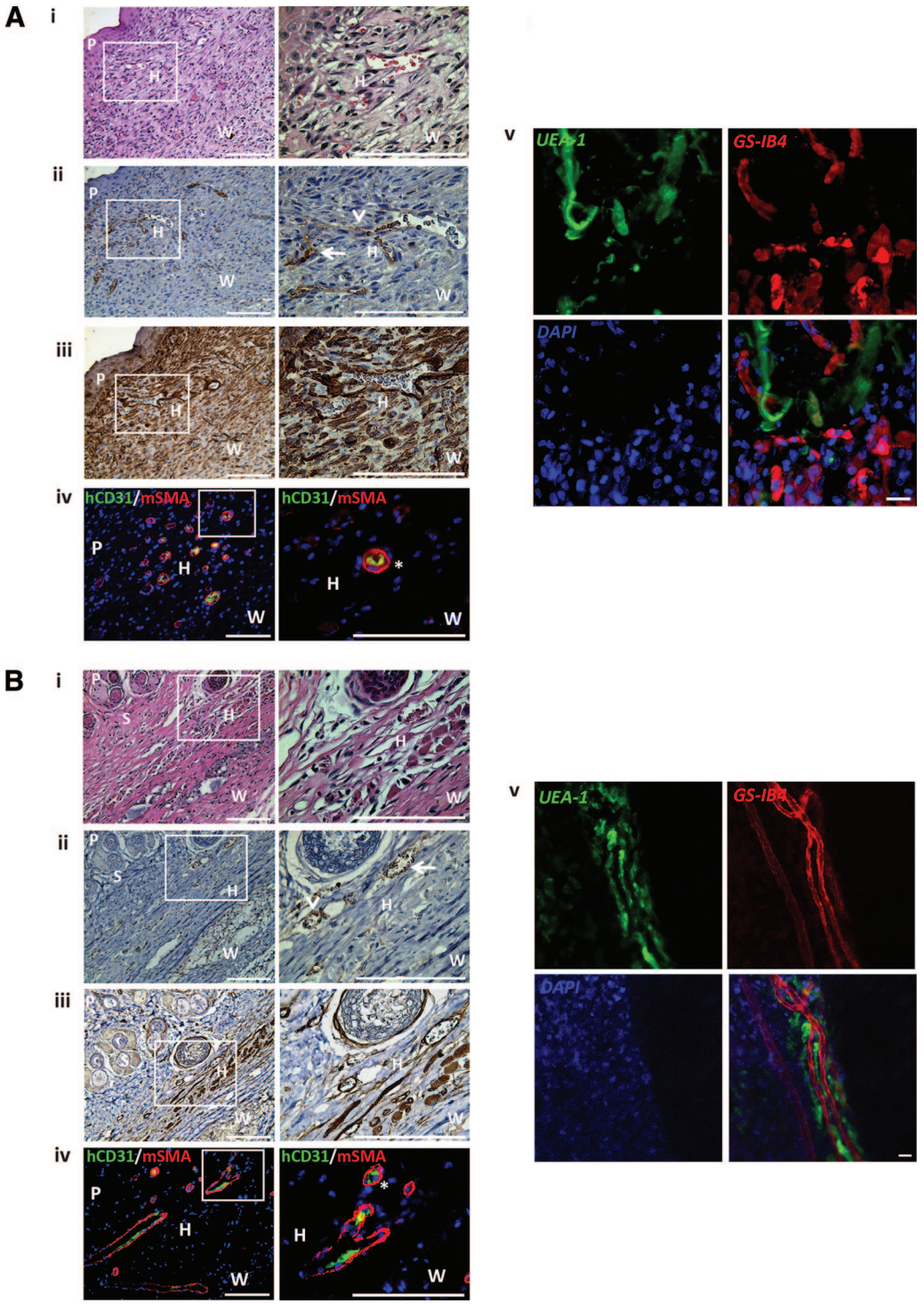

Figure 4. Wound analysis during inflammation to proliferation periods (days 11–14). After the treatment with human microvascular constructs, the wounds were analyzed at day 11 **(A)** and day 14 **(B)**. Representative images of H&E-stained histological sections **(Ai, Bi)**, immunohistochemistry for human CD31 staining **(Aii, Bii)** (brown; counterstain in blue), immunohistochemistry for mouse α-SMA staining **(Aiii, Biii)** (brown; counterstain in blue), and immunofluorescence staining for human CD31 (green) and mouse α-SMA **(Aiv, Biv)** (red; nuclei in blue) are shown. High magnifications of the boxed areas are shown on the right. **(Av, Bv):** Representative confocal images of preperfused explant with fluorescein-conjugated *UEA-1* lectin in green; *GS-IB4* lectin in red; nuclei in blue. Human microvasculatures alone (some indicated by arrows), chimeric human and mouse vessels (some indicated by arrowheads), and human microvasculatures wrapped by mouse smooth muscle cells (some indicated by asterisk) are shown. Scale bars = 100 μm. Abbreviations: DAPI, 4′,6-diamidino-2-phenylindole; H, hydrogel; mSMA, mouse α-smooth muscle actin; P, epidermis; S, sebaceous gland; W, wound.

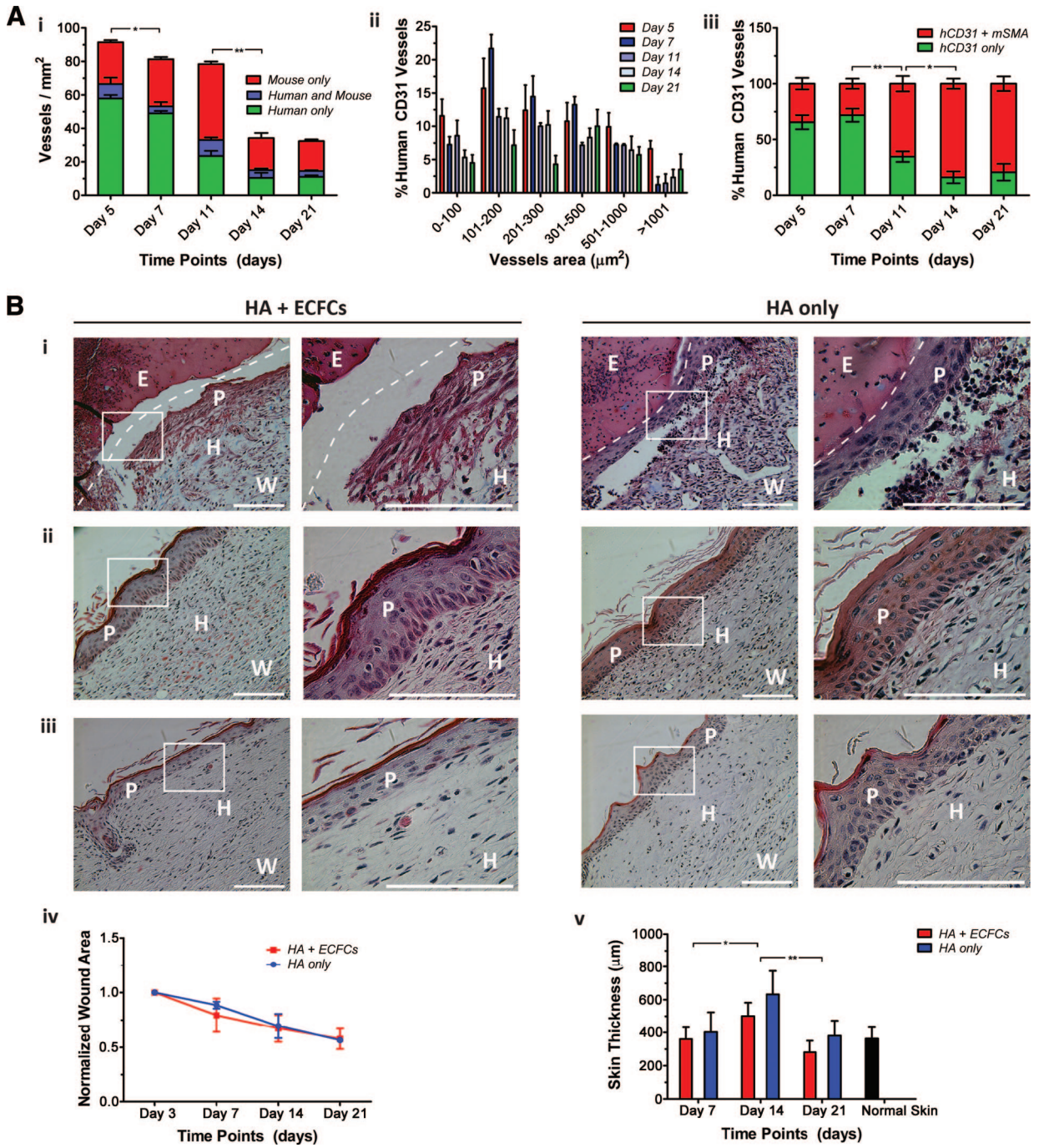

Figure 5. Vessel quantification and analysis of the healing skin. **(Ai):** Types of vessels found in the wound area during the healing periods: human-only vessel, chimeric human and mouse vessels, and mouse-only vessel. **(Aii):** Size distribution of human CD31-positive vessels in the wound area during the healing periods. **(Aiii):** Percentage of human CD31-positive vessels covered by mouse smooth muscle cells in the wound area during the healing periods. **(B):** Masson's trichrome staining of the wound area at day 7 **(Bi)**, day 14 **(Bii)**, and day 21 **(Biii)** after treatment with HA hydrogel containing human vasculature (left) and HA hydrogels alone, without the addition of any growth factors (right). High magnifications of the boxed areas are shown on the right. The dotted white line indicates the border between the eschar and the growing new skin. Scale bars = 100 μm. **(Biv, Bv):** Quantification of the normalized wound area **(Biv)** and the skin thickness during the healing process **(Bv)**. Significance levels are set at $p < .05$ (*) and $p < .01$ (**). Abbreviations: E, eschar; ECFCs, endothelial colony-forming cells; H, hydrogel; HA, hyaluronic acid; mSMA, mouse α-smooth muscle actin; P, epidermis; W, wound.

human CD31 (Fig. 4Aii), whereas most of them were positive for α-SMA (Fig. 4Aiii). Some of the human vessels were wrapped by mouse SMCs (Fig. 4Aiv). We detected a larger number of mouse vessels and an increase in chimeric human-mouse vessels in the wound area, as shown in the perfusion study (Fig. 4Av). As remodeling of the wound started (day 14), a sharp regression occurred in the vessels surrounding the wound area, whereas some were maintained around the new, growing hair follicles and associated sebaceous glands (Fig. 4Bi). Some of the human vessels were retained around the

healed wound area and the matured mouse vessels (Fig. 4Bii–4Bv). As the wound reached the later remodeling stage (day 21), human CD31-positive vessels were retained near the healed wound area (supplemental online Fig. 2B).

Vasculature Characteristics in the Treated Wounds

To better understand the cellular dynamic of the implanted human vascular network constructs, quantification analysis of the vasculature during the healing process was performed. A gradual decrease in the overall number of vessels was observed in the wound area as the healing progressed, with a sharp decrease of 50% on day 14. The number of vessels seemed to stabilize by the end of the healing process at day 21 at $\sim$40 vessels per mm^2. During the first week of healing, the majority of the vessels in the treated wound area were human (60.26 $\pm$ 1.78%), but then during the second week of healing, the host vasculature overtook them (56.10 $\pm$ 9.04%; Fig. 5Ai). The number of the chimeric vessels, which contained both human and mouse cells, remained relatively constant through the healing process (5–10 vessels per mm^2; Fig. 5Ai). Analyzing the human blood vessels, we found that they increased in size around the wound area during the proliferation period (days 5–7), then they regressed (days 11–14) and were further stabilized late in remodeling period (day 21), whereas the majority of microvessels (i.e., with a vessel area less than 200 μm^2) remained (Fig. 5Aii). Through the transitions from inflammation to proliferation (days 5–7), approximately 28.21 $\pm$ 4.57% of human vessels were covered by mouse SMCs. This percentage increased through the transitions from inflammation to proliferation (days 11–14), reaching 79.35 $\pm$ 6. 51% at the late remodeling stage (day 21; Fig. 5Aiii). When HA hydrogels alone (without the addition of any growth factors) were used to treat the wound, similar kinetics were observed during the healing process: an early proliferation of the vessels, followed by regression and stabilization to maintain the majority of the microvessels (supplemental online Fig. 4).

Skin Regeneration

During the inflammation period (day 3), the wound started to close and decreased in size as the healing progressed through the proliferation (day 7) and remodeling (day 14) stages, leading to complete closure on day 21 (supplemental online Fig. 1). During the proliferation period (day 7), the eschar started to detach from the wound, and a new epithelium developed with a normal maturation pattern on top of the wound; this held true for both wounds treated with HA hydrogels containing human vasculatures and those treated with HA hydrogels alone, without the addition of any growth factors (Fig. 5Bi). As the wound reached the remodeling period (day 14), the skin tissue thickened with some collagen deposition in the dermis (Fig. 5Bii). By the late remodeling period (day 21), the skin thickness slightly decreased and exhibited more organized epithelial cells (Fig. 5Biii). We could not detect a significant difference between the kinetics of the wound closures in wounds treated with HA alone or in wounds treated with HA containing human vessels (Fig. 5Biv; supplemental online Fig. 1). Quantification of skin thickness revealed that it grew thicker through the beginning of the remodeling period (day 14) but got thinner as remodeling progressed (day 21), becoming comparable to the thickness of normal skin (Fig. 5Bv; supplemental online Fig. 5). We found no significant difference in skin thickness between wounds treated with HA only and those treated with HA having human vasculatures from ECFCs (Fig. 5Bv).

Discussion

Tissue engineering requires an understanding of vascularized tissue construct kinetics as they integrate with their host vasculature [3, 12, 42]. This study showed that engineered human vascular networks using ECFCs in HA hydrogels can rapidly integrate with host vasculature during the healing process in a third-degree burn model. As previously reported in a subcutaneous model [20], here we also show that rapid degradation by host macrophages is crucial to allow host tissue and vessel ingrowth into the HA hydrogels. No significant differences exist between the degradation kinetics of HA hydrogel alone (without the addition of any growth factors) and HA containing human vessels: in both treatments, the hydrogels mostly degraded by day 3. The observed degradation kinetics here occurred faster than our previously reported photocrosslinked dextran hydrogels, where macrophages recruited at day 5, and they degraded most of the gels by day 7 [29]. The rapid degradation in these HA hydrogels was mainly facilitated by the MMP-sensitive peptide crosslinker within the HA hydrogels and occurred independently of the encapsulated ECFCs.

Angiogenesis and neovascularization appeared in the wound area at the onset of the proliferation and remodeling stages [24]. Once the macrophages allowed host vessels to grow into the hydrogels and the wounds reached the proliferation period (day 5), localization of the human and mouse vessels was observed around the wound area. Since burn wounds stimulate a rapid angiogenic response, the integration kinetics observed here agreed with a different wound healing model where human vessels began to integrate with the host vessels at day 3 when a Matrigel plug was used [12] and at day 7 when collagen and fibrin gels were used [42]. In the middle of the proliferation period (day 7), mouse host vessels grew into the wound area, integrating with the human vascular networks to support the regenerating tissue. This was indicated by the increased number and size of the chimeric vessels that contain both human and mouse vessels at day 11, demonstrating the functionality and integration of the engineered human vascular networks with the host vasculatures. At this stage, the percentage of human vessels that were covered by mouse SMCs also increased. It should be noted that growth in mouse vasculature in the wounded area may occur either by the recruitment of vasculature to the wound area (angiogenesis) or by the recruitment of bone-marrow endothelial progenitors (vasculogenesis) [25, 38]. Once the wound reaches the remodeling period (day 14), vessels started to regress; some, including the human vessels, were retained near the hair follicles and associated sebaceous glands. Late in the remodeling period (day 21), most of the microvessels, human and mouse, were stabilized and retained in the healed skin tissue. The majority of the implanted vasculatures retained in the healed tissue were human vessels that were wrapped by mouse SMCs. These observations suggest that future study could use perivascular cells, which have physical [43, 44] and paracrine effects [45], to improve the durability of the engineered vasculatures [9, 13]. The kinetics of vessel proliferation to support the new, growing tissue followed by regression at the remodeling stage is the hallmark of the wound-healing process [25, 38, 45] and can also be observed in wounds treated with HA hydrogels alone. Vessel

regression is a normal part of wound healing, and the kinetics that we observed here agreed with other studies demonstrating that skin graft vascularization requires regulated regression and replacement of the vascular networks by both angiogenesis and vasculogenesis [25, 38, 45]. In fact, the goal is not to have permanently increased vascularization, but to accelerate the healing process and to promote healing without excessive scar formation [22, 29].

Once the wound reached the remodeling period (day 14), the skin layer thickened with regenerating epithelial cells. By the end of this period (day 21), the skin became thinner, with more organized epithelial cells and collagen layer, and started to resemble the structure of healthy skin [29]. We did not observe significantly different healing outcomes for wounds treated only with HA hydrogel compared with those treated with HA hydrogel having human vessels. Our previous study demonstrated that photopolymerized dextran hydrogels alone, without the addition of growth factors, cytokines, or cells, promoted rapid neovascularization and complete skin regeneration with appendages (hair follicles and sebaceous glands) [29]. The current study shows that HA hydrogels (either alone or with human vascular networks) achieved a more rapid hydrogel degradation (on day 3 compared with day 5 with dextran) but did not result in comparable accelerated skin regeneration. The difference in final outcomes between dextran and HA hydrogels may be attributed to the unique chemistry and degradation behavior of the dextran hydrogels, which promote appropriate healing kinetics and epidermal homeostasis [28], resulting in full skin regeneration [29], whereas the HA hydrogel may degrade quickly to allow human vessels to integrate with the host vasculature but do not promote complete skin regeneration with appendages. It is also important to note that, to accommodate the human ECFC xenograft implantation, we used nude mice, which may have different skin and hair regeneration potential than the nonimmunocompromised mice used for the experiments with the dextran hydrogels.

Conclusion

Collectively, our findings suggest that human vasculature engineered from ECFCs can integrate with the host vessels in a deep third-degree burn model. Moreover, this study demonstrated that HA hydrogels that support the precise formation of human vasculature in vitro can be successfully delivered to the site of injury, where they can survive and integrate with the host vasculature. The kinetics of human vasculature growth followed the healing progression of the deep wound and regressed with the overall vessel pruning around the healed tissue. Insights gained from this study may help to improve vascularization of tissue-engineered constructs, as well as offer improvements in tissue regeneration for patients with various dermal wounds and ischemic conditions.

Acknowledgments

We thank Dr. Guoming Sun for helping with the wound-healing procedure and Fransisca Puspa Dewi for her creative illustrations in the figures. This research was partially funded by an American Heart Association Scientist Development grant (to S.G.) and NIH Grant R01-HL107938.

Author Contributions

D.H.-P.: conception and design, collection and assembly of data, data analysis and interpretation, manuscript writing; Y.-I.S. and A.W.: collection of data, data analysis and interpretation; K.F.-T.: collection of data; S.K.: provision of study material; J.A.B.: conception and design, manuscript writing; C.S.: data analysis and interpretation, manuscript writing; S.G.: conception and design, financial support, data analysis and interpretation, manuscript writing, final approval of manuscript.

Disclosure of Potential Conflicts of Interest

The authors indicate no potential conflicts of interest.

References

1 Rafii S, Lyden D. Therapeutic stem and progenitor cell transplantation for organ vascularization and regeneration. Nat Med 2003; 9:702–712.

2 Dvir T, Kedem A, Ruvinov E et al. Prevascularization of cardiac patch on the omentum improves its therapeutic outcome. Proc Natl Acad Sci USA 2009;106:14990–14995.

3 Koffler J, Kaufman-Francis K, Shandalov Y et al. Improved vascular organization enhances functional integration of engineered skeletal muscle grafts. Proc Natl Acad Sci USA 2011; 108:14789–14794.

4 Caspi O, Lesman A, Basevitch Y et al. Tissue engineering of vascularized cardiac muscle from human embryonic stem cells. Circ Res 2007;100:263–272.

5 Nör JE, Peters MC, Christensen JB et al. Engineering and characterization of functional human microvessels in immunodeficient mice. Lab Invest 2001;81:453–463.

6 Levenberg S, Rouwkema J, Macdonald M et al. Engineering vascularized skeletal muscle tissue. Nat Biotechnol 2005;23:879–884.

7 Wang ZZ, Au P, Chen T et al. Endothelial cells derived from human embryonic stem cells form durable blood vessels in vivo. Nat Biotechnol 2007;25:317–318.

8 Ferreira LS, Gerecht S, Shieh HF et al. Vascular progenitor cells isolated from human embryonic stem cells give rise to endothelial and smooth muscle like cells and form vascular networks in vivo. Circ Res 2007;101: 286–294.

9 Melero-Martin JM, De Obaldia ME, Kang SY et al. Engineering robust and functional vascular networks in vivo with human adult and cord blood-derived progenitor cells. Circ Res 2008;103:194–202.

10 Au P, Daheron LM, Duda DG et al. Differential in vivo potential of endothelial progenitor cells from human umbilical cord blood and adult peripheral blood to form functional long-lasting vessels. Blood 2008; 111:1302–1305.

11 Critser PJ, Kreger ST, Voytik-Harbin SL et al. Collagen matrix physical properties modulate endothelial colony forming cell-derived vessels in vivo. Microvasc Res 2010; 80:23–30.

12 Kang K-T, Allen P, Bischoff J. Bioengineered human vascular networks transplanted into secondary mice reconnect with the host vasculature and re-establish perfusion. Blood 2011;118:6718–6721.

13 Au P, Tam J, Fukumura D et al. Bone marrow derived mesenchymal stem cells facilitate engineering of long-lasting functional vasculature. Blood 2008;111:4551–4558.

14 Lutolf MP, Hubbell JA. Synthetic biomaterials as instructive extracellular microenvironments for morphogenesis in tissue engineering. Nat Biotechnol 2005;23:47–55.

15 Hanjaya-Putra D, Gerecht S. Mending the failing heart with a vascularized cardiac patch. Cell Stem Cell 2009;5:575–576.

16 Phelps EA, Landázuri N, Thulé PM et al. Bioartificial matrices for therapeutic vascularization. Proc Natl Acad Sci USA 2010;107: 3323–3328.

17 Webber MJ, Tongers J, Newcomb CJ et al. Supramolecular nanostructures that mimic VEGF as a strategy for ischemic tissue repair. Proc Natl Acad Sci USA 2011;108:13438–13443.

18 Chen Y-C, Lin R-Z, Qi H et al. Functional human vascular network generated in photocrosslinkable gelatin methacrylate hydrogels. Adv Funct Mater 2013;22:2027–2039.

19 Moon JJ, Saik JE, Poché RA et al. Biomimetic hydrogels with pro-angiogenic properties. Biomaterials 2010;31:3840–3847.

20 Hanjaya-Putra D, Bose V, Shen Y-I et al. Controlled activation of morphogenesis to generate a functional human microvasculature in a synthetic matrix. Blood 2011;118:804–815.

21 Hanjaya-Putra D, Wong KT, Hirotsu K et al. Spatial control of cell-mediated degradation to regulate vasculogenesis and angiogenesis in hyaluronan hydrogels. Biomaterials 2012;33:6123–6131.

22 Gurtner GC, Werner S, Barrandon Y et al. Wound repair and regeneration. Nature 2008;453:314–321.

23 Tibbs MK. Wound healing following radiation therapy: A review. Radiother Oncol 1997;42:99–106.

24 Singer AJ, Clark RAF. Cutaneous wound healing. N Engl J Med 1999;341:738–746.

25 Capla JM, Ceradini DJ, Tepper OM et al. Skin graft vascularization involves precisely regulated regression and replacement of endothelial cells through both angiogenesis and vasculogenesis. Plast Reconstr Surg 2006;117:836–844

26 Bhora FY, Dunkin BJ, Batzri S et al. Effect of growth factors on cell proliferation and epithelialization in human skin. J Surg Res 1995;59:236–244.

27 Martin P. Wound healing: Aiming for perfect skin regeneration. Science 1997;276:75–81.

28 Blanpain C, Fuchs E. Epidermal homeostasis: A balancing act of stem cells in the skin. Nat Rev Mol Cell Biol 2009;10:207–217.

29 Sun G, Zhang X, Shen Y-I et al. Dextran hydrogel scaffolds enhance angiogenic responses and promote complete skin regeneration during burn wound healing. Proc Natl Acad Sci USA 2011;108:20976–20981.

30 Kung EF, Wang F, Schechner JS. In vivo perfusion of human skin substitutes with microvessels formed by adult circulating endothelial progenitor cells. Dermatol Surg 2008;34:137–146.

31 Schechner JS, Nath AK, Zheng L et al. In vivo formation of complex microvessels lined by human endothelial cells in an immunodeficient mouse. Proc Natl Acad Sci USA 2000;97:9191–9196.

32 Shepherd BR, Enis DR, Wang F et al. Vascularization and engraftment of a human skin substitute using circulating progenitor cell-derived endothelial cells. FASEB J 2006;20:1739–1741.

33 Hirschi KK, Ingram DA, Yoder MC. Assessing identity, phenotype, and fate of endothelial progenitor cells. Arterioscler Thromb Vasc Biol 2008;28:1584–1595.

34 Yoder MC, Mead LE, Prater D et al. Redefining endothelial progenitor cells via clonal analysis and hematopoietic stem/progenitor cell principals. Blood 2007;109:1801–1809.

35 Hanjaya-Putra D, Yee J, Ceci D et al. Vascular endothelial growth factor and substrate mechanics regulate in vitro tubulogenesis of endothelial progenitor cells. J Cell Mol Med 2010;14:2436–2447.

36 Khetan S, Katz JS, Burdick JA. Sequential crosslinking to control cellular spreading in 3-dimensional hydrogels. Soft Matter 2009;5:1601–1606.

37 Khetan S, Burdick JA. Patterning network structure to spatially control cellular remodeling and stem cell fate within 3-dimensional hydrogels. Biomaterials 2010;31:8228–8234.

38 Zhang X, Wei X, Liu L et al. Association of increasing burn severity in mice with delayed mobilization of circulating angiogenic cells. Arch Surg 2010;145:259–266.

39 Sun G, Shen Y-I, Kusuma S et al. Functional neovascularization of biodegradable dextran hydrogels with multiple angiogenic growth factors. Biomaterials 2011;32:95–106.

40 Robertson D, Savage K, Reis-Filho J et al. Multiple immunofluorescence labelling of formalin-fixed paraffin-embedded (FFPE) tissue. BMC Cell Biol 2008;9:13.

41 Sun G, Shen Y-I, Ho CC et al. Functional groups affect physical and biological properties of dextran-based hydrogels. J Biomed Mater Res A 2010;93:1080–1090.

42 Cheng G, Liao S, Kit Wong H et al. Engineered blood vessel networks connect to host vasculature via wrapping-and-tapping anastomosis. Blood 2011;118:4740–4749.

43 Vo E, Hanjaya-Putra D, Zha Y et al. Smooth-muscle-like cells derived from human embryonic stem cells support and augment cord-like structures in vitro. Stem Cell Rev 2010;6:237–247.

44 Wanjare M, Kuo F, Gerecht S. Derivation and maturation of synthetic and contractile vascular smooth muscle cells from human pluripotent stem cells. Cardiovasc Res 2013;97:321–330.

45 Skardal A, Mack D, Kapetanovic E et al. Bioprinted amniotic fluid-derived stem cells accelerate healing of large skin wounds. Stem Cells Translational Medicine 2012;1:792–802.

See www.StemCellsTM.com for supporting information available online.